Colloids and Surfaces B: Biointerfaces 83 (2011) 83–90

Contents lists available at ScienceDirect

Colloids and Surfaces B: Biointerfaces

journal homepage: www.elsevier.com/locate/colsurfb

N,*N*′-Carbonyldiimidazole-mediated functionalization of superparamagnetic nanoparticles as vaccine carrier

Jenny Ho[a,*], Fatin M. Nawwab Al-Deen[a], Aswan Al-Abboodi[a], Cordelia Selomulya[a], Sue D. Xiang[b], Magdalena Plebanski[b], Gareth M. Forde[a]

[a] Department of Chemical Engineering, Monash University, Clayton 3800, VIC, Australia
[b] Department of Immunology, Central Clinical School, Faculty of Medicine, Nursing and Health Sciences, Monash University, Melbourne 3004, VIC, Australia

ARTICLE INFO

Article history:
Received 29 July 2010
Received in revised form 29 October 2010
Accepted 1 November 2010
Available online 5 November 2010

Keywords:
N,*N*′-Carbonyldiimidazole
Superparamagnetic nanoparticles
Magnetite
Particulate vaccine carrier

ABSTRACT

Particulates with specific sizes and characteristics can induce potent immune responses by promoting antigen uptake of appropriate immuno-stimulatory cell types. Magnetite (Fe_3O_4) nanoparticles have shown many potential bioapplications due to their biocompatibility and special characteristics. Here, superparamagnetic Fe_3O_4 nanoparticles (SPIONs) with high magnetization value (70 emu g^{-1}) were stabilized with trisodium citrate and successfully conjugated with a model antigen (ovalbumin, OVA) via *N*,*N*′-carbonyldiimidazole (CDI) mediated reaction, to achieve a maximum conjugation capacity at approximately 13 μg μm^{-2}. It was shown that different mechanisms governed the interactions between the OVA molecules and magnetite nanoparticles at different pH conditions. We evaluated as-synthesized SPION against commercially available magnetite nanoparticles. The cytotoxicity of these nanoparticles was investigated using mammalian cells. The reported CDI-mediated reaction can be considered as a potential approach in conjugating biomolecules onto magnetite or other biodegradable nanoparticles for vaccine delivery.

1. Introduction

Vaccines have been used for treatment and control for a range of infectious diseases, and it is imperative to develop novel vaccine formulations to induce the right type of protective immunity against pathogens and diseases such as malaria, cancers, acquired immunodeficiency syndrome (AIDS) and others. The first generation vaccines were based on the use of inactivated or live-attenuated immunogenic pathogens; however, possible reversions to virulent forms and adverse side effects like inflammation have impeded the rapid development of this type of vaccines [1]. Second generation vaccines have focused on the development of sub-unit vaccines (*i.e.* protein antigens or recombinant protein components) along with the rapid advances in genomics and proteomics. Nevertheless, these vaccines too require immuno-stimulating agents to optimize the desired immune response via selective targeting of the vaccines to antigen presenting cells (APCs) [2]. Nanoparticles in the viral size range offer distinct advantages including high intracellular uptake, while CD4 and CD8 T cells as well as antibodies could be elicited through antigen attached onto the nanoparticle surfaces [3]. Professional APCs such as dendritic cells (DCs) are initiators and modulators of immune responses, enabling antigens to be processed through both major histocompatibility complex (MHC) class I and II pathways. Therefore, the delivery of therapeutic molecules such as protein and peptides to DCs, and the activation of antigen presenting pathway are critical in the development of effective vaccines [4].

Previous studies have proven the concept that particle size is crucial for immunogenicity and influence the internalization of nanoparticles by APCs [5]. Particles with sizes close to virus (20–200 nm) are preferentially taken up by DCs through endocytosis, while larger particle (0.5–5 μm) are primarily taken up by macrophages via phagocytosis [5,6]. Notably, nanoparticles of 40–50 nm in diameter can induce potent CD8 T-cell and Th1 responses, while sub-micron particles promote Th2 responses [5,7]. Adjuvants such as latex, polystyrene, gold and silica [8] are commonly examined as antigen carriers for induction of immunity; however, they are not biodegradable. In recent years, liposomes [9,10], biodegradable polymers [11], immunostimulating complexes (ISCOMs) [12,13], particulates and virus-like particles (VLPs) *etc.* [8] have also been developed as antigen carriers. It was found that covalently coupled antigen-carrier system stimulated higher cellular and humoral responses than physically adsorption approach especially for localization to dendritic cells in draining lymph nodes, which is attributed to higher antigen to nanoparticles

* Corresponding author. Tel.: +61 3 9905 4682; fax: +61 3 9905 5686.
E-mail addresses: jenny.ho@eng.monash.edu.au, jenny.ho.jh@gmail.com (J. Ho).

0927-7765/$ – see front matter © 2010 Elsevier B.V. All rights reserved.
doi:10.1016/j.colsurfb.2010.11.001

ratio and can prevent the losses of antigen from nanoparticle's surface during physiological circulation [5]. Regardless of these efforts, the challenge remains to obtain carrier particles within the narrow size range, of high stability and adjuvanticity, and with a good safety profile.

Magnetic iron oxide nanoparticles with a unique combination of small size, biodegradable properties, and processability have been widely used experimentally for a variety of technological applications, ranging from data recording and magnetic seals in motors to magnetic resonance imaging (MRI) and hyperthermia for cancer treatment. For most biomedical applications, uniform physical and chemical properties such as high magnetic moment, high magnetic susceptibility and narrow size distribution within sub-100 nm are crucial [14]. In particular, superparamagnetic behavior which provides a rapidly changing magnetic state and zero coercivity can help reduce the extent of aggregation especially during intravenous administration, as no magnetism remains in the absence of external magnetic field. In the last decade, magnetite (Fe_3O_4) or its oxidized form, maghemite (γ-Fe_2O_3) with single domains of about 5–20 nm in diameter are by far the most promising candidates with good biocompatibility [15]. In addition, the surfaces of magnetite and maghemite could be modified with numerous coatings and are suitable for further functionalization by the attachment of various bioactive molecules [14]. Most of all, application of an external magnetic field can be used to position the magnetic iron oxide nanoparticles to a localized site.

The possibilities to conjugate biomolecules onto magnetic iron oxide nanoparticles are numerous, mostly relying on surface functionalities. The majority of these studies have employed silanization to introduce a variety of ideal anchorages onto the surface of magnetic iron oxide nanoparticles for covalent binding of specific molecules [14,16]; and conventional crosslinking molecules such as carbodiimide, glutaraldehyde, *N*-hydroxysuccinimidyl-3-(2-pyridyldithio)-propionate (SPDP) or *N*,*N*′ methylene *bis* acrylamide (MBA) that are commonly used for immobilization [14]. However, these methods require multiple steps which resulted in a complicated and time-consuming procedure. The ideal scenario is to have generic and homogenous binding sites that could selectively bind the desired molecules and preserve their native structure. Furthermore, formation of large aggregates, low conjugation efficiency, low stability, and inconsistent conjugate characteristics are common obstacles in conjugates preparation.

In this study, we report a facile method for the optimal conjugation of ovalbumin (OVA) as a model antigen onto magnetite nanoparticles (MNPs) for use as particulate vaccines. In general, iron oxide samples exhibit a high degree of surface hydrophilicity and contain approximately a closed-packed hydroxyl concentration of 6–10 molecules nm^{-1} [17]. The activating agent and the intermediate reactive group of activation strategies for hydroxylic particles are mostly susceptible to hydrolysis; therefore, the activations are frequently done under non-aqueous conditions. One convenient way is to use *N*,*N*′-carbonyldiimidazole (CDI), a highly reactive carboxylating agent that contains two acylimidazole leaving groups, to form reactive carbonyl groups on the hydroxyl particles. This conjugate reagent has been successfully used in peptide synthesis [18] and also in the immobilization of enzyme and affinity ligands in chromatography matrix [19]. Herein, we investigate the feasibility of this CDI-mediated mechanism in conjugating OVA onto two different types of magnetite nanoparticles (MNPs)-commercially available and self-synthesized superparamagnetic iron oxide nanoparticles (SPIONs); and the associated optimal conjugation conditions and problems that may arise. The obtained magnetite samples immobilized with OVA are highly dispersed in aqueous solution with promising conjugation efficiency. In addition, the cytotoxicity profiles of these formulations toward mammalian cells were also evaluated to assess the potential use in biomedical applications.

2. Materials and methods

2.1. Materials

The magnetite (iron (II, III) oxide nanopowder, Fe_3O_4, < 50 nm particle size), ovalbumin (Grade III), trisodium citrate dihydrate ($C_6H_5Na_3O_7 \cdot 2H_2O$), sodium hydroxide (NaOH), sodium phosphate (Na_2HPO_4), sodium acetate (CH_3COONa), dimethylsulphoxide (DMSO), 3-(4,5-dimethylthiazol-2-yl)-2,5-diphenyltetrazolium bromide (MTT), phosphate buffered saline (PBS), foetal calf serum, bicinchoninic acid (BCA) assay kit and other associated reagent grade chemicals were purchased from Sigma–Aldrich (Sydney, Australia). RPMI 1640 medium (GIBCO), 0.05% trypsin–EDTA, L-glutamine and penicillin/streptomycin were supplied by Invitrogen (Carlsbad, CA). Other materials include ammonium persulphate, Tris–HCl (pH 8.8), sodium dodecyl sulphate (SDS), acrylamide/bisacrylamide and tetramethylenediamine (TEMED) were obtained from Silenus Laboratories (Melbourne, Australia). Fe (III) chloride hexahydrate ($Fe\,Cl_3 \cdot 6H_2O$) was purchased from Ajax Finechem (NSW, Australia) and Fe (II) sulphate ($FeSO_4 \cdot 7H_2O$) was supplied by Ajax Chemicals (Sydney, Australia). Rare earth (neodymium) circular disc magnets (diameter 12 mm × thickness 10 mm) were purchased from Aussie Magnet Company Ptd. Ltd. Other materials include Tetrahydrofuran (RCI LabScan Ltd., Thailand), Spectra/Por 7 dialysis tubing with 25 kDa molecular weight cut-off (MWCO) (Spectrum Laboratories Inc., USA) and Ethanolamine (BDH Chemicals Ltd., USA).

2.2. Synthesis of superparamagnetic iron oxide nanoparticles (SPIONs)

In order to achieve a narrow size distribution, superparamagnetic iron oxide nanoparticles (SPIONs) were prepared by alkaline co-precipitation of ferric and ferrous chlorides in aqueous solution, using trisodium citrate ($Na_3C_6H_5O_7$) as an electrostatic stabilizer. The three carboxylate groups of trisodium citrate have strong affinity to Fe^{3+} and will render the surface negatively charged [20]. Therefore, the magnetite cores can be sterically separated, thus preventing the single crystals to agglomerate into larger crystals. Moreover, these highly dispersed SPIONs can be further functionalized for different bioapplications [21]. The preparation method was modified from co-precipitation of ferrous and ferric ion solutions (1:2 molar ratios) [22] with the chemical reaction given in Eq. (1):

$$Fe^{2+} + 2Fe^{3+} + 8OH^- \rightarrow Fe_3O_4 + 4H_2O \quad (1)$$

Briefly, iron salts, ferric chloride (0.005 mol) and ferrous sulphate (0.0025 mol) were dissolved in 20 ml deionized (DI) water and the precipitation was performed by dropwise addition of iron salt solutions to the mixed sodium hydroxide solution (20 ml, 1.5 M, including 0.005 mol trisodium citrate) under vigorous stirring (1500 rpm) for 1 h at 80 °C in a nitrogen (N_2) atmosphere. Oxygen was removed from the solution by flowing N_2 gas through the reaction medium in a closed system before the synthesis reaction. The resulting black precipitates were collected from the solution by applying an external magnet, which were then washed four times: first with DI water, twice with ethanol, and finally with DI water to remove any excess ions and salts from the suspension. The washed precipitate was then dispersed in 20 ml DI water. The concentration of the magnetite nanoparticles was approximately 8 mg ml^{-1}. The resulting nanoparticles were stored at 4 °C for future use.

2.3. Characterization of magnetite nanoparticles

2.3.1. Dynamic light scattering and electron microscopy

The synthesized SPIONs and commercially available magnetite (Sigma) were characterized by various analytical techniques. The hydrodynamic diameter distribution and zeta potential were determined directly after the preparation by using the Zetasizer Nano ZS (Malvern Instruments Ltd., UK), which utilizes dynamic light scattering (DLS) to determine the size distribution. The dry nanoparticle size and morphology were analyzed using scanning electron microscopy (SEM). Samples were placed directly on a silicon chip wafer (ProSciTech, Qld, Australia) and dried at 50 °C for 30 min. The dried samples were then coated with 1 nm of platinum, and characterized with a JEOL JSM-7001F field emission scanning electron microscope (FESEM), which was operated at an accelerating voltage of 15 kV. Transmission electron microscopy (TEM) images of the SPIONs were obtained using a Hitachi H7500 TEM instrument at an accelerating voltage of 120 kV.

2.3.2. Structural and magnetic properties analysis

X-ray powder diffraction (XRD) measurements were performed with a Philips PW 1140/90 diffractometer using Cu Kα radiation at a scan rate of $1^\circ\,min^{-1}$ from 5° to 60° with a step size of 0.02° in determining crystallinity and phase of the magnetite samples. Fourier transform infrared (FTIR) spectra of the MNPs, dispersed in KBr and pelletized, were obtained using PerkinElmer Spectrum 100 Series FT-IR spectrometer in a wave number ranging from 4000 to 400 cm^{-1} with a resolution accuracy of 4 cm^{-1} under ambient condition. The specific values for the saturation magnetization were obtained using vibrating sample magnetometer (VSM, Princeton Applied Research, model ISS) operating at room temperature. A known weight of the samples was placed into the VSM sample holder and a maximum magnetic field of approximately 5 kOe was used. The magnetization values under 5 kOe were normalized to the mass of samples to yield the M_s (emu g^{-1}).

2.4. Functionalization of magnetite nanoparticles with ovalbumin

5 mg ml^{-1} of MNPs were washed sequentially with 10 ml each of DI water, THF–DI water (2:8, 4:6, 6:4, and 8:2, v/v) and finally with anhydrous THF for several repeated washes to eliminate any remaining traces of water. The MNPs were precipitated with the help of external magnet and re-suspended thoroughly with ultrasonic bath between each wash. Carbonyldiimidazole (CDI) was then added into the suspension at a concentration of 50 mg ml^{-1} and reacted at 700 rpm mixing in a shaker for 2 h at room temperature. The MNPs were washed three times with THF to remove excess CDI and reaction by-products, and subsequently three quick washes were performed with ice-cold 0.1 M sodium phosphate buffer (pH 8.5) to remove traces of THF. The MNPs were re-suspended in 0.1 M sodium phosphate buffer (pH 8.5) at a final concentration of 10 mg ml^{-1}, and OVA (Grade III) was then dissolved in the suspension to ensure a final OVA concentration ranging from 0.5 to 10 mg ml^{-1}. The conjugation mixture was incubated at 4 °C and 700 rpm mixing for 24 h. The resulting MNPs were separated from supernatant of the final conjugation mixture using external magnet after 24 h, and the supernatant was collected for BCA analysis to determine the amount of un-conjugated OVA according to manufacturer's instructions. The amount of OVA bound onto the MNPs was calculated from the difference between the initial OVA added and the remaining amount of OVA in the supernatant. The collected MNPs were then washed 3 times in 0.1 M sodium phosphate buffer (pH 8.5) to remove any un-reacted OVA. 5 ml of 0.1 M of enthanolamine in the buffer was then added to the MNPs to quench any remaining active imidazole carbamate groups for another 2 h, followed by 3 washes in the 0.1 M sodium phosphate buffer and finally dialysis overnight in 0.1 M phosphate buffered saline (PBS, pH 7.4) using 25 kDa MWCO dialysis tubing. The OVA conjugated MNPs were stored at 4 °C for subsequent analysis and use. Procedures above were repeated using 0.1 M of sodium acetate buffer (pH 5) instead of 0.1 M sodium phosphate. The scheme for the overall functionalization of magnetite (Fe_3O_4) nanoparticles is similar to a previously reported reaction [19] and is shown in Fig. 1.

2.5. Determination of protein bonding stability to the magnetite nanoparticles

The specific binding stability of OVA onto the MNPs can be determined using sodium dodecyl sulphate polyacrylamide gel electrophoresis (SDS-PAGE). An aliquot of OVA conjugated MNPs were loaded onto the non-reducing SDS-PAGE gel and electric field was applied. The MNPs themselves do not migrate into the gel and remain in the loading well; however, protein (e.g. OVA) not covalently coupled but physically adsorbed will migrate into the gel when subjected to the electric field. Therefore, the stability of specific bonding can be observed from protein bands after gel staining.

2.6. Cytotoxicity assay

The cytotoxicity of various formulations prepared with MNPs was evaluated by determining the cell viability of COS-7 cell line (SV-40 transformed African Green Monkey kidney fibroblast cells) after co-cultured with the MNPs using MTT assay. MTT reagent (3-(4,5-dimethylthiazol-2-yl)-2,5-diphenyltetrazolium bromide) is a

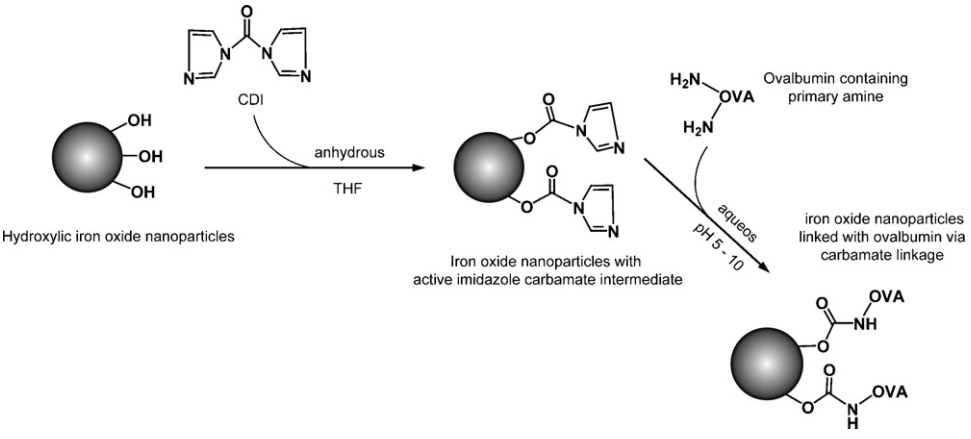

Fig. 1. Schematic representation of the preparation route of OVA-conjugated magnetite nanoparticles through CDI mediated reaction.

yellow and water soluble tetrazolium salt that is reduced to insoluble purple formazan in the living cells by active mitochondrial reductase enzyme. The MTT assay is a non-radioactive colorimetric test to quantify the cell cytotoxicity, proliferation or viability as a function of mitochondrial activity in the living cells, while dead cells lose their ability to reduce tetrazolium salt. Therefore, an organic solvent like dimethylsulphoxide (DMSO) was used to dissolve formazan crystals formed, and then quantified by measuring the absorbance at wavelengths of 570 nm and 690 nm. This obtained value would correlate with the amount of viable cells. The different formulations were sterilized with UV radiation for 30 min prior MTT assay. 100 μl of COS-7 cells were seeded in a 96 well flat-bottom plate at a density of 2×10^4 cells per well and incubated in a humidified 37 °C incubator with 5% CO_2. After 24 h, 100 μl of various MNPs formulations (0.1 mg ml^{-1}) in phosphate buffered saline (PBS, pH 7.4) were added to each well, apart from the control wells where 100 μl of PBS were added instead. The cells were further cultured for 24 h. 5 μl of MTT solution at a concentration of 5 mg ml^{-1} (in PBS, pH7.4) was then added to each well and further incubated at 37 °C with 5% CO_2. The medium was removed after 4 h and the cells were rinsed 2 times with PBS. 100 μl of DMSO were then added to each well and incubated for another 1 h to solubilize the formazan crystals. After 1 h incubation, the optical absorbance of each well was measured at wavelength of 570 nm and 690 nm instantaneously using a microplate reader (Magellan, Tecan, Austria). The cell viabilities (%) relative to control were calculated as follows:

$$\text{Viability}\ \ (\%) = \left(\frac{\text{means absorbance of sample}}{\text{means absorbance of control}}\right) \times 100\%$$

3. Results and discussion

3.1. Magnetite nanoparticles

The synthesis and characterization of superparamagnetic iron oxide nanoparticles (SPIONs) have been extensively reviewed in literature [14,15]. The particle size and surface charge are critical for their phagocytosis or endocytosis rate, toxicity, plasma half-life-period, plasma proteins opsonisation, and velocity of cytoplasmic movement, with all these characteristics important for optimal outcomes in biomedical applications [14]. In our study, the self-synthesized SPIONs were well-defined nanoparticles of about 15 ± 3 nm in diameter from SEM and TEM images (Fig. 2a and b), while the commercially available MNPs were 34 ± 5 nm (Fig. 2c). The mean hydrodynamic diameter (D_H) of the nanoparticles, as measured by dynamic light scattering, were around 40 ± 5 nm for the self-synthesized SPIONs and ~700 nm for commercial MNPs (Fig. 3). The relatively narrow size distribution as measured by dynamic light scattering implied that the self-synthesized SPIONs were highly stable in suspension, with the presence of trisodium citrate providing highly effective steric stabilization around the single crystals to prevent agglomeration during synthesis [20,21]. Moreover, a high stirring rate (up to 1500 rpm) has been employed in the co-precipitation process, contributing to smaller and more uniform sizes since higher amount of energy was transferred to the suspension during synthesis. The self-synthesized SPIONs exhibited highly negative zeta potential (-50 ± 3 mV). On the contrary, the size distribution in suspension for the commercially available MNPs displayed a wide distribution, indicating severe agglomeration of nanoparticles perhaps due to the co-existence of remanence and magnetic inter-particle interactions. In this case, the commercially available MNPs being slightly ferromagnetic, have stronger magnetic dipole-dipole attractions between the particles, so that even in the absence of any external magnetic field, the magnetostatic interactions between particles can cause agglomeration [23]. On the other hand, the smaller size SPIONs displayed superparamagnetism, without any remanence magnetization in the absence of magnetic field.

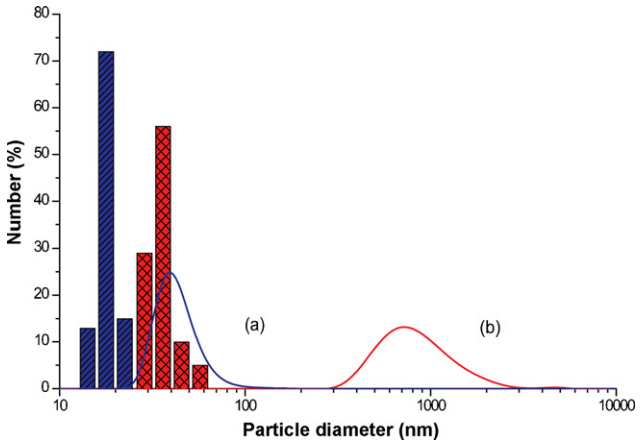

Fig. 3. The hydrodynamic diameter (D_H) of (a) SPIONs (blue) and (b) commercially available MNP (red) are represented by line graphs, in comparison to sizes observed through FESEM images (blue and red bars, respectively). (For interpretation of the references to color in this figure legend, the reader is referred to the web version of the article.)

Fig. 4 shows the magnetization curves of self-synthesized SPIONs and commercial magnetite under the maximum applied field of 5 kOe. The magnetization values were normalized to the mass of samples to yield the specific magnetization, M_S expressed in electromagnetic units per gram (emu g^{-1}). The SPIONs exhibited M_S of around 70 emu g^{-1} with no hysteresis curve, signifying its superparamagnetic behavior. When the magnetic field was removed, their magnetization reached zero, indicating that the synthesized SPIONs were single crystal domains. Their thermal energy was sufficient to overcome the magnetic anisotropic energy barrier and

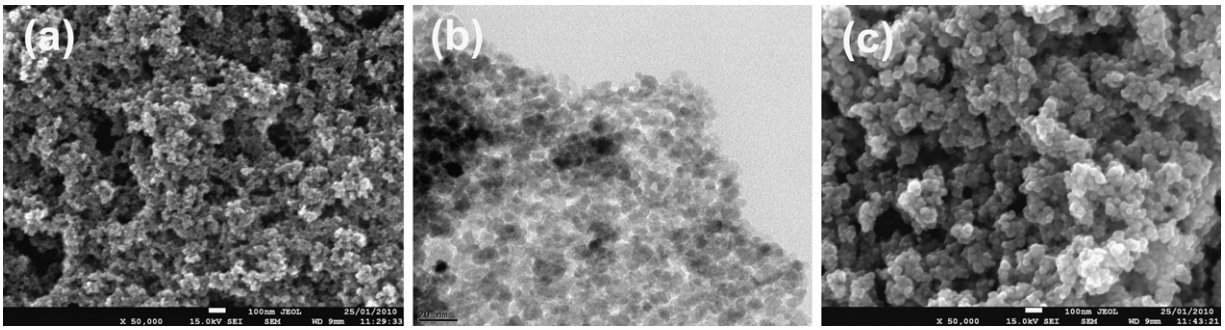

Fig. 2. (a) FESEM and (b) TEM images for self-synthesized superparamagnetic iron oxide nanoparticles (SPIONs); (c) FESEM image of commercially available magnetite nanoparticles (MNP).

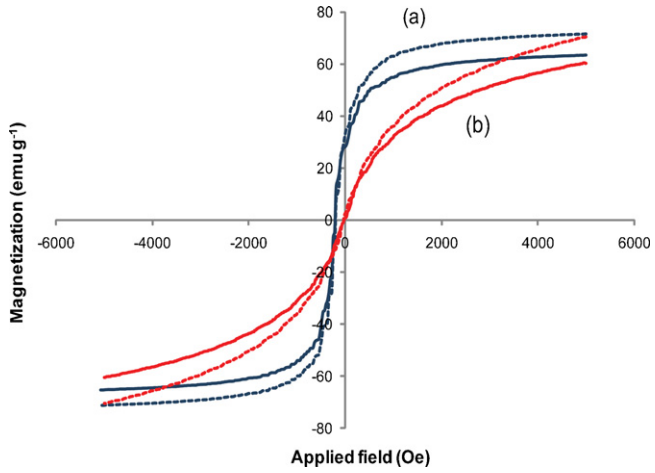

Fig. 4. Room temperature magnetization curves of (a) SPIONs (blue) and (b) commercially available MNP (red) before (- - -) and after (—) conjugated with OVA. (For interpretation of the references to color in this figure legend, the reader is referred to the web version of the article.)

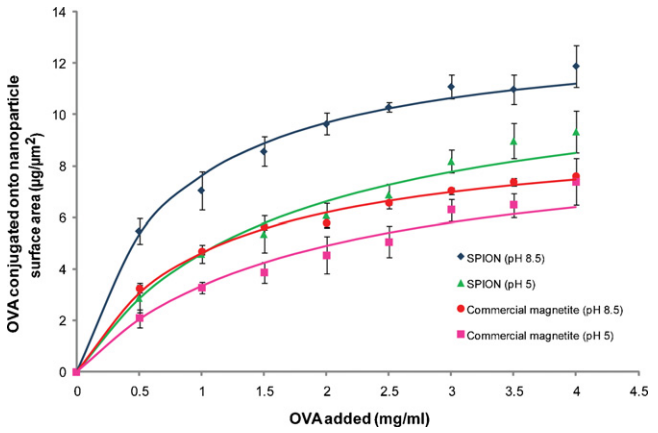

Fig. 6. Conjugation capacity of OVA to SPIONs and commercially available MNP in both pH 5 and pH 8.5 conditions, and their fitting with Langmuir model (line graphs). These results are the mean of three experiments ± SD (standard deviation).

invert the magnetic spin direction, leading to a net zero magnetization [24]. The M_s of commercial magnetite was recorded as ~75 emu g^{-1}; however, a slight hysteresis was observed at the curve, indicating that the particles were partly ferromagnetic. The X-ray diffraction patterns of both self-synthesized SPIONs and commercial magnetite are given in Fig. 5. Six characteristic peaks for Fe_3O_4 ($2\theta = 30.3°$, 35.6°, 43.3°, 53.7°, 57.3° and 62.9°) as marked by their indices were noted for both samples [25]. These peaks revealed that both samples were pure Fe_3O_4 with spinel structure, although the synthesized SPIONs have slightly low and broadening diffraction peaks due to decreasing of crystalline structure in the presence of trisodium citrate [21].

3.2. Functionalization of magnetic iron oxide nanoparticles with OVA

The surfaces of Fe_3O_4 are populated with hydroxyl groups (–OH) and provide the basis for further functionalization. Besides enabling controlled interaction with targeted biological species, better aqueous dispersion and biocompatibility are among the ultimate aims of successful surface functionalization. Ideally, the bio-functionalization should facilitate effective stabilization of the

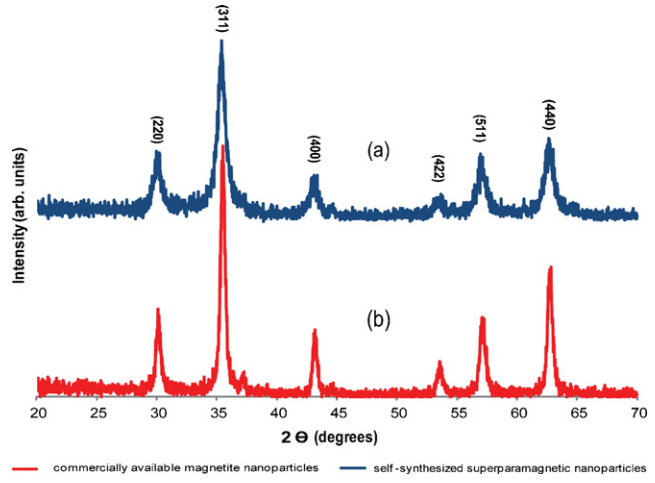

Fig. 5. XRD spectra of (a) SPIONs (blue) and (b) commercially available MNP (red). (For interpretation of the references to color in this figure legend, the reader is referred to the web version of the article.)

biomolecules in their biologically relevant conformations on the nanoparticles surface. To utilize the self-synthesized SPIONs as particulate vaccines and comparing them to the commercial particles, *N*,*N*′-carbonyldiimidazole (CDI) was used to activate the hydroxyl groups of both samples for conjugation of ovalbumin (OVA). The conjugation capacities of both samples at two pH conditions (pH 5 and 8.5) are shown in Fig. 6. In general, at higher pH condition (pH 8.5), the data fitted well to a typical Langmuir isotherm, implying a monolayer and strong interaction between OVA molecules and the CDI functionalized MNPs surfaces [26]. Nevertheless, at low pH condition (pH 5), the isotherm shows a sharp initial rise, suggesting fast adsorption kinetics although the data did not fit well with the monolayer Langmuir isotherm at higher OVA concentration. We postulate that different mechanisms are governing the interactions between the OVA molecules and MNPs in different pH conditions. Commonly, CDI activates the hydroxyl groups to form imidazolyl carbamate of high reactivity (Fig. 1). At elevated pH (pH 8.5), nucleophilic attack of free amino groups in OVA upon these reactive intermediates is stimulated to greatly improve immobilization. Attack by the amine group will then release the imidazole, resulting in the formation of a one-carbon length and stable *N*-alkyl carbamate linkage [19]. The isoelectric point (p*I*) of OVA is ~4.8 from zeta potential measurement, rendering the OVA with a net positive charge below the p*I* value and a net negative charge above the p*I* value; whereas the p*I*s for self-synthesized SPIONs and commercial magnetite were around pH 6 and 6.5, respectively (data not shown). At pH 5, the net charge of OVA molecules is low; therefore the dominant mechanism responsible for the interaction between OVA and MNP is the attraction of the non-polar side chains of the amino acid residues on the surface of OVA to the reactive intermediate electrophiles of MNP. This phenomenon is analogous to neutralized precipitation and will promote closer packing of OVA on the MNP surface. When the loaded OVA are in excess, there is a high possibility of multiple adsorptions on the MNP surface as shown in Fig. 6. Frequently, the greatest coupling yields for proteins to CDI-activated systems occur in an environment of at least one pH unit above their pI values especially in alkaline buffers [19]. In Fig. 6, the monolayer conjugation capacity fitting with Langmuir model was calculated using equation:

$$q^* = \frac{q_{max} C^*}{K_D + C^*} \quad (2)$$

where K_D is the Langmuir coefficient, C^* is the concentration of OVA solution, q_{max} is the maximum monolayer conjugation capacity and q^* is the amount of OVA attached on the MNP. K_D and q_{max} values obtained for SPIONs and commercial magnetite in differ-

Table 1
Summary of maximum monolayer conjugation capacity and Langmuir coefficient obtained in different pH conditions for both SPIONs and commercial available MNP.

Sample	q_{max} (μg μm^{-2})	K_D (mM)
SPION		
pH 8.5	13.3	0.0166
pH 5	11.9	0.0353
Commercial magnetite		
pH 8.5	9.0	0.0199
pH 5	9.2	0.0391

ent pH conditions of this study are summarized in Table 1. The K_D values displayed by OVA in elevated pH condition indicated higher bonding strength than at pH 5, suggesting that the bonding at lower pH might not be necessarily in the form of chemical bonding. To prove the type and stability of bonding between OVA and the MNP, SDS-PAGE was employed to investigate the interaction pattern. According to Fig. 7, the absence of a protein band for both self-synthesized SPIONs and commercial magnetite conjugation mixtures at pH 8.5 clearly indicated that the OVA molecules were covalently bound onto the nanoparticles. Contrarily, a dim protein band for the self-synthesized SPIONs conjugation mixtures at pH 5 after gel staining implied that only parts of the OVA molecules were adsorbed onto the nanoparticles. The mild treatment for protein and electric field during SDS-PAGE would not break the extensive covalent bonding, but would affect the physical interactions such that the primary interaction at low pH was most possibly via physical rather than chemical bonding. The FTIR spectra of both the self-synthesized SPIONs and commercial magnetite before and after CDI-based conjugation with OVA are shown in Fig. 8a and b, respectively. The appearance of the characteristic absorption band for Fe_3O_4 at around 590 cm^{-1} in the spectra for both samples before conjugation; the attenuation of the band; and the presence of amide bands upon the attachment of OVA denoted the successful OVA

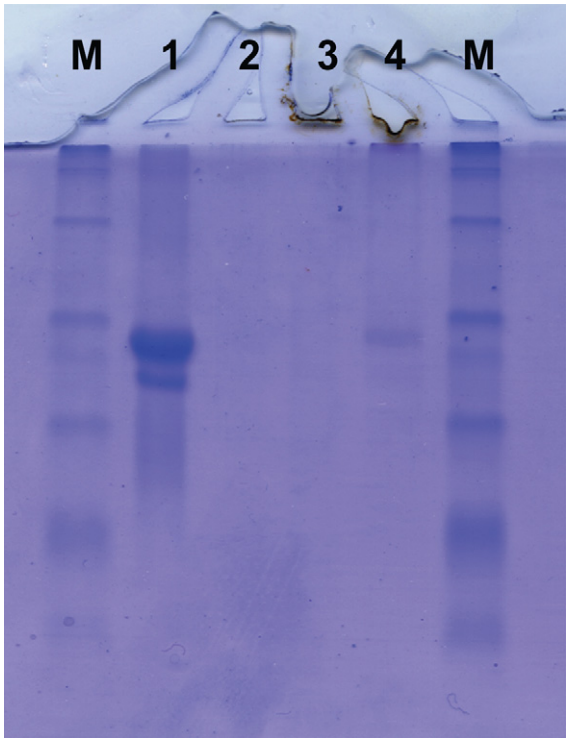

Fig. 7. Analysis of specific binding of OVA using SDS-PAGE. Lane M, protein marker; lane 1, native ovalbumin; lane 2, conjugation mixture of commercially available MNP at pH 8.5; lane 3, conjugation mixture of SPIONs at pH 8.5; lane 4, conjugation mixture of SPIONs at pH 5.

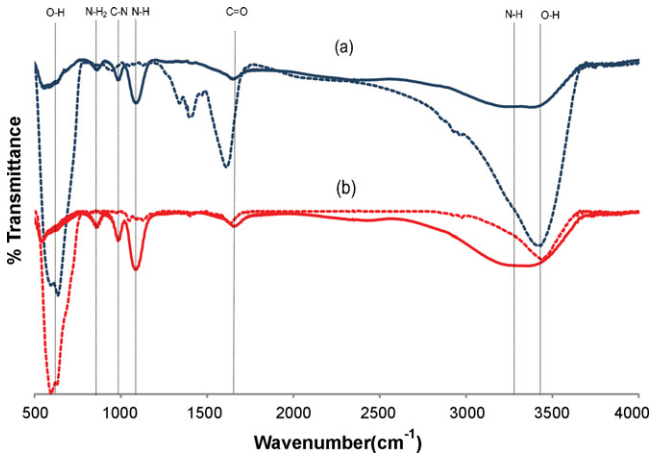

Fig. 8. FTIR spectra of (a) SPIONs (blue) and (b) commercially available MNP (red) before (—) and after (- - -) conjugated with OVA. (For interpretation of the references to color in this figure legend, the reader is referred to the web version of the article.)

conjugation onto both surfaces of MNPs. The M_s of both samples conjugated with OVA were slightly decreased (Fig. 4), with the SPIONs retaining their superparamagnetism. Surprisingly, the average hydrodynamic diameters and the size distributions for both SPIONs and commercially available MNP conjugated with OVA have shifted towards smaller size ranges (Fig. 9). This could possibly due to the attachment of OVA on the surfaces of MNPs that minimized the magnetostatic interactions between individual nanoparticles, thus stabilizing them in suspension. In addition, the shelf-stability of both SPIONs and commercially available MNP conjugated with OVA had increased to over 4 weeks and 1 week, respectively; in comparison to the naked SPIONs (~2 weeks) and commercially available MNP (<1 h).

3.3. Cytotoxicity studies

The MTT assay was used to investigate the toxicity of Fe_3O_4 nanoparticles to the cultured cells. This assay relies on the mitochondrial activity of cells and represents their metabolic activity with viability > 80% recognized as good biocompatibility [24]. The influences of naked and OVA-conjugated MNPs on the COS-7 cells viability after 24 h incubation are shown in Fig. 10. The results clearly indicated that self-synthesized SPIONs were more favourable than commercial magnetite for the prolifera-

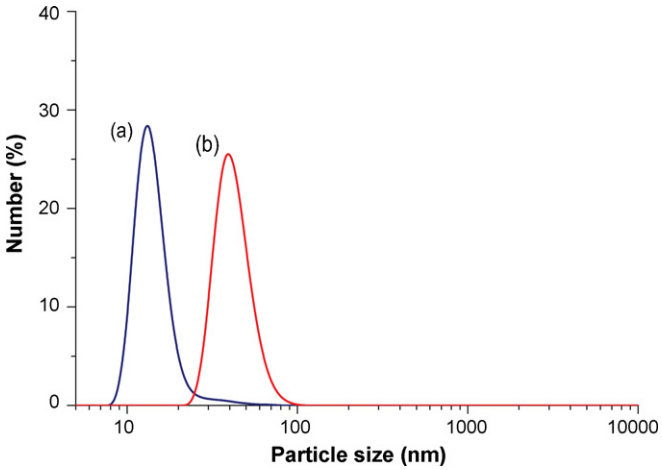

Fig. 9. The hydrodynamic diameter (D_H) of (a) SPIONs (blue) and (b) commercially available MNP (red) after conjugation with OVA. (For interpretation of the references to color in this figure legend, the reader is referred to the web version of the article.)

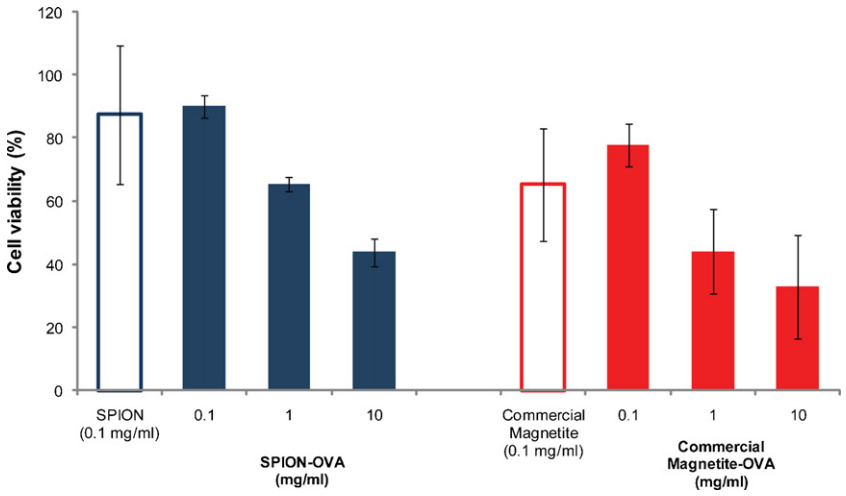

Fig. 10. Assessment of viability of COS-7 cells incubated with medium containing native (bars with no fill) SPIONs (blue or left) and commercially available MNP (red or right) at 0.1 mg ml^{-1}, and also conjugation mixture (bars with fill) at several concentrations. These results are the mean of three experiments ± SD (standard deviation). (For interpretation of the references to color in this figure legend, the reader is referred to the web version of the article.)

tion/viability of COS-7 cells, with generally more than 80% viability before and after OVA conjugation when incubated with the conjugation mixture at 0.1 mg ml^{-1}. Magnetic nanoparticles were found to cause minimal toxicity due to the possibility of causing oxidative DNA lesions in cultured human epithelial cells [27]. The presence of citrate groups on the surface of self-synthesized SPIONs increased their negative zeta potential and dispersion in aqueous solution, subsequently promoting their biocompatibility with cells [21,28]. The cytotoxicity effect of the MNPs became more predominant with increasing concentration; and the cell viability reached as low as 33% at MNP concentration of 10 mg ml^{-1}. One possible explanation for this significant reduction in cell viability may be that these MNP generated more pronounced damages to the cell membrane structure as a result of multiple endocytosis and accelerated apoptosis. The concentration of 0.1 mg ml^{-1} with high biocompatibility is higher than the normal dosage for particulate vaccine that usually given in the micrograms range. Nonetheless, in few instances of our study, the cell viability achieved more than 100% relative to control (data not shown) and can be due to the nutrient effect of the iron oxide [29]. The low toxicity profile of MNP further demonstrated its potential biomedical applications, particularly as particulate vaccines in this case.

4. Conclusions

In summary, we have demonstrated the feasibility to conjugate OVA as a model antigen onto self-synthesized superparamagnetic iron oxide nanoparticles (SPIONs) with comparison to commercially available magnetite nanoparticles, via a facile CDI-based strategy, with the objective to use as particulate vaccines for targeting dendritic cells. The functionalization was best carried out in the alkaline conditions and the conjugation capacity fitted well with the monolayer Langmuir model. The nanosized OVA-functionalized SPIONs particles have high magnetic responsivity (>60 emu g^{-1}), excellent dispersibility and shelf stability in suspension, and low cytotoxicity (>80% viability). The combination of these properties suggested that they could be ideal candidates as vaccine carriers, with further works currently being carried out to induce antibody responses *in vivo*.

Acknowledgements

This work is supported by Australian Research Council Discovery Project Grant (DP0986357). The authors would like to thank Professor Ross Coppel from the Department of Microbiology, Monash University in allowing the use of their facility for part of this work.

References

[1] I. Amanna, M.K. Slifka, Public fear of vaccination: separating fact from fiction, Viral Immunol. 18 (2005) 307–315.
[2] Y.J. Kwon, S.M. Standley, S.L. Goh, J.M.J. Frechet, Enhanced antigen presentation and immunostimulation of dendritic cells using acid-degradable cationic nanoparticles, J. Control. Release 105 (2005) 199–212.
[3] J.P.Y. Scheerlinck, S. Gloster, A. Gamvrellis, P.L. Mottram, M. Plebanski, Systemic immune responses in sheep, induced by a novel nano-bead adjuvant, Vaccine 24 (2006) 1124–1131.
[4] M.F Lipscomb, B.J. Masten, Dendritic cells: immune regulators in health and disease, Physiol. Rev. 82 (2002) 97–130.
[5] T. Fifis, A. Gamvrellis, B. Crimeen-Irwin, G.A. Pietersz, J. Li, P.L. Mottram, I.F.C. McKenzie, M. Plebanski, Size-dependent immunogenicity: therapeutic and protective properties of nano-vaccines against tumors, J. Immunol. 173 (2004) 3148–3154.
[6] L. Pelkmans, Secrets of caveolae- and lipid raft-mediated endocytosis revealed by mammalian viruses, Biochim. Biophys. Acta: Mol. Cell Res. 1746 (2005) 295–304.
[7] P.L. Mottram, D. Leong, B. Crimeen-Irwin, S. Gloster, S.D. Xiang, J. Meanger, R. Ghildyal, N. Vardaxis, M. Plebanski, Type 1 and 2 immunity following vaccination is influenced by nanoparticle size: formulation of a model vaccine for respiratory syncytial virus, Mol. Pharm. 4 (2007) 73–84.
[8] S.D. Xiang, K. Scalzo-Inguanti, G. Minigo, A. Park, C.L. Hardy, M. Plebanski, Promising particle-based vaccines in cancer therapy, Expert Rev. Vaccines 7 (2008) 1103–1119.
[9] A.C. Allison, G. Gregoria, Liposomes as immunological adjuvants, Nature 252 (1974) 252–1252.
[10] Y. Perrie, A.R. Mohammed, D.J. Kirby, S.E. McNeil, V.W. Bramwell, Vaccine adjuvant systems: enhancing the efficacy of sub-unit protein antigens, Int. J. Pharm. 364 (2008) 272–280.
[11] M.E.C. Lutsiak, D.R. Robinson, C. Coester, G.S. Kwon, J. Samuel, Analysis of poly(D,L-lactic-co-glycolic acid) nanosphere uptake by human dendritic cells and macrophages in vitro, Pharm. Res. 19 (2002) 1480–1487.
[12] I.G. Barr, A. Sjolander, J.C. Cox, ISCOMs and other saponin based adjuvants, Adv. Drug Deliv. Rev. 32 (1998) 247–271.
[13] C.D. Skene, P. Sutton, Saponin-adjuvanted particulate vaccines for clinical use, Methods 40 (2006) 53–59.
[14] A.K. Gupta, M. Gupta, Synthesis and surface engineering of iron oxide nanoparticles for biomedical applications, Biomaterials 26 (2005) 3995–4021.
[15] T. Neuberger, B. Schopf, H. Hofmann, M. Hofmann, B. von Rechenberg, Superparamagnetic nanoparticles for biomedical applications: possibilities and limitations of a new drug delivery system, J. Magn. Magn. Mater. 293 (2005) 483–496.
[16] I. Koh, X. Wang, B. Varughese, L. Isaacs, S.H. Ehrman, D.S. English, Magnetic iron oxide nanoparticles for biorecognition: evaluation of surface coverage and activity, J. Phys. Chem. B 110 (2006) 1553–1558.
[17] F.J. Micale, D. Kiernan, A.C. Zettlemoyer, Characterization of the surface-properties of iron oxides, J. Colloid Interface Sci. 105 (1985) 570–576.
[18] R. Paul, G.W. Anderson, *N,N′*-carbonyldiimidazole, a new peptide forming reagent, J. Am. Chem. Soc. 82 (1960) 4596–4600.
[19] M.T.W. Hearn, 1,1′-Carbonyldiimidazole-mediated immobilization of enzymes and affinity ligands, Methods Enzymol. 135 (1987) 102–117.

[20] S. Campelj, D. Makovec, M. Drofenik, Preparation and properties of water-based magnetic fluids, J. Phys.: Condens. Matter 20 (2008) 204101.
[21] J. Liu, Z.K. Sun, Y.H. Deng, Y. Zou, C.Y. Li, X.H. Guo, L.Q. Xiong, Y. Gao, F.Y. Li, D.Y. Zhao, Highly water-dispersible biocompatible magnetite particles with low cytotoxicity stabilized by citrate groups, Angew. Chem. Int. Ed. 48 (2009) 5875–5879.
[22] R. He, X.G. You, J. Shao, F. Gao, B.F. Pan, D.X. Cui, Core/shell fluorescent magnetic silica-coated composite nanoparticles for bioconjugation, Nanotechnology 18 (2007) 315601.
[23] M. Mahmoudi, A. Simchi, A.S. Milani, P. Stroeve, Cell toxicity of superparamagnetic iron oxide nanoparticles, J. Colloid Interface Sci. 336 (2009) 510–518.
[24] A.K. Gupta, S. Wells, Surface-modified superparamagnetic nanoparticles for drug delivery: preparation, characterization, and cytotoxicity studies, IEEE Trans. Nanobiosci. 3 (2004) 66–73.
[25] Y.-C. Chang, D.-H. Chen, Preparation and adsorption properties of monodisperse chitosan-bound Fe_3O_4 magnetic nanoparticles for removal of Cu(II) ions, J. Colloid Interface Sci. 283 (2005) 446–451.
[26] H. Schmidt-Traub, Preparative Chromatography of Fine Chemicals and Pharmaceutical Agents, Wiley-VCH, Weinheim, 2005.
[27] H.L. Karlsson, P. Cronholm, J. Gustafsson, L. Moller, Copper oxide nanoparticles are highly toxic: a comparison between metal oxide nanoparticles and carbon nanotubes, Chem. Res. Toxicol. 21 (2008) 1726–1732.
[28] Z.G.M. Lacava, R.B. Azevedo, E.V. Martins, L.M. Lacava, M.L.L. Freitas, V.A.P. Garcia, C.A. Rebula, A.P.C. Lemos, M.H. Sousa, F.A. Tourinho, M.F. Da Silva, P.C. Morais, Biological effects of magnetic fluids: toxicity studies, J. Magn. Magn. Mater. 201 (1999) 431–434.
[29] D. Fischer, Y.X. Li, B. Ahlemeyer, J. Krieglstein, T. Kissel, In vitro cytotoxicity testing of polycations: influence of polymer structure on cell viability and hemolysis, Biomaterials 24 (2003) 1121–1131.